https://doi.org/10.5194/egusphere-2026-1317
Preprint. Discussion started: 8 April 2026

Maximum Certainty Principle applied to rainfall modelling and regionalisation in Ecuador

Franklin Aparicio Beltrán Vega[1 2], Jhoan Alexander Beltrán Valarezo[1]

[1] IDD Consultores - IDD Research, Earth Sciences, Quito, Ecuador
[2] Secretaría de Educación Superior, Ciencia, Tecnología e Innovación (SENESCYT), Quito, Ecuador

Correspondence to: Franklin A. Beltrán (fabeltran@iddresearch.org)

Abstract. This study introduces the Maximum Certainty Principle (PCM, from the Spanish "Principio de Certeza Máxima") as a variational framework for the probabilistic modelling of storm events and its application to the regionalisation of extreme rainfall. First, the PCM is developed and applied in the Metropolitan District of Quito through the Storm Information Model (MIT-Q), which represents the intra-event temporal structure using a truncated exponential formulation derived from the PCM variational functional. Within MIT-Q, event maximum precipitation (PRE) and event duration (DT) are modelled using Weibull and truncated exponential distributions, respectively. Stochastic simulations equivalent to 500 years of rainfall were performed, calibrated against Intensity–Duration–Frequency (IDF) curves from the Quito-Observatory station and validated at four additional stations within an area of approximately 2500 km². Results indicate that extreme rainfall intensities with durations shorter than 2 h are statistically independent of daily intensities, and that the structural separation between PRE and DT improves the representation of short-duration extremes. Second, the structural insights obtained at the local scale are extended to the existing national rainfall regionalisation framework of Ecuador. A scaling factor (φ) associated with the potential number of rainfall bursts, representing the dynamics of local winds and the growth of storm cells, is introduced, enabling the derivation of Potential Intensity–Duration–Frequency (IDFP) curves that remain useful under sparse observation network conditions, such as those of the Ecuadorian network. The proposed approach integrates theoretical development, local validation, and regional scaling within a structural probabilistic framework for the analysis of extreme rainfall.
Keywords. Maximum certainty principle, MIT-Q, storms, rainfall regionalisation, Ecuador IDF.

1 Introduction

The search for invariants is a central strategy for understanding complex systems: when it is not possible to describe every individual detail, a conserved quantity may condense collective information that remains stable despite variation in its components (Lévy-Leblond, 2002). In physics, this idea acquires a precise formulation by linking symmetries with conservation laws: Noether's theorem states that, under appropriate variational hypotheses, the continuous invariance of the action leads to conserved quantities (Noether, 1918; Noether and Tavel, 2005; Butterfield, 2006; Halder et al., 2018). Moreover, the Noetherian framework distinguishes between proper and improper divergence relations. Conceptually, this

https://doi.org/10.5194/egusphere-2026-1317
Preprint. Discussion started: 8 April 2026

reflects the separation between geometric differential identities—valid independently of the equations of motion—and genuine conservation laws that govern the system dynamics. This distinction is relevant when interpreting invariant properties or conserved quantities that emerge from general mathematical structures rather than from a specific physical mechanism (Kosmann-Schwarzbach, 2011, pp. 57–62).

In a probabilistic setting, the notion of conservation is reformulated by explicitly incorporating the information associated with event occurrence. In information theory, the surprise of observing an outcome with probability p is quantified by −log p, and its expectation defines Shannon entropy (Shannon, 1948). In statistical inference, the Maximum Entropy Principle selects the distribution that preserves exactly the information contained in the constraints, without adding unsupported structure; Jaynes (1957) interprets it as a method of reasoning consistent with the available information.

On this basis, the PCM proposes an alternative criterion for selecting distributions and trajectories: rather than optimizing only disorder (entropy) or goodness of fit to the data, it maximises a composite functional that integrates (i) a structural term called the Knowledge Potential (PC) and (ii) an informational term associated with event unexpectedness. Within this framework, the invariant quantity, maximum Certainty (ℵmax), is expressed as a single value that compactly integrates the contribution of the Knowledge Potential and the informational term. This value synthesises the balance between structure and uncertainty over a finite interval (Beltrán, 2023).

In urban hydrology and tropical mountain environments, this perspective is pertinent because intense rainfall exhibits marked spatiotemporal variability and an intra-event structure that directly influences runoff, erosion, and flooding. Classical literature shows that, in many intense storms, a substantial fraction of the total volume can be concentrated in the first quartiles of the event, leading to asymmetric temporal patterns (Huff, 1967). In parallel, Rodríguez-Iturbe et al. (1987) discuss stochastic models for the temporal variation of rainfall intensity at a fixed point. In a first family, storm events originate according to a Poisson process, and the total intensity is defined as the sum of contributions active over time. In a second, more complex family, storms also arise from a Poisson process, but each storm generates a cluster of rain cells, which allows the representation of more than one temporal scale through clustered point processes (Rodríguez-Iturbe et al., 1987).

For hydraulic design, the synthesis of precipitation extremes is operationally expressed through Intensity–Duration–Frequency (IDF) curves, which relate the maximum intensity associated with a given return period to event duration; their construction and fitting have been widely discussed in the hydrological literature (Koutsoyiannis et al., 1998).

In the Andean context, estimating IDF curves faces additional challenges associated with complex topography, strong elevation gradients, and the orographic influence on atmospheric circulation, which generate pronounced spatial variability in precipitation (Garreaud, 2009; Escobar-González et al., 2022). In Ecuador, the National Institute of Meteorology and Hydrology (INAMHI) has developed national studies aimed at determining equations for maximum precipitation intensities by fitting distributions and estimating intensities for different return periods at multiple stations across the country (Guachamin, 2019). However, these studies do not explicitly document the application of a formal probabilistic regionalisation scheme that integrates information from multiple sites under statistical homogeneity criteria and enables joint estimation of extreme quantiles, such as those proposed by Hosking and Wallis (1997).

https://doi.org/10.5194/egusphere-2026-1317
Preprint. Discussion started: 8 April 2026

Within this framework, the objective of this article is to apply the PCM to the probabilistic modelling and regional synthesis of rainfall in Ecuador, using available pluviograph and IDF information as a basis. In particular, the following question is posed: can a probabilistic invariant $\aleph_{max}$ be defined from IDF information that synthesizes the interaction between temporal structure and uncertainty, enabling (i) the reinterpretation of INAMHI empirical parameters in structural terms, (ii) the identification of characteristic temporal patterns in precipitation events, and (iii) the proposal of an operational extension—termed Potential IDF curves—that contributes to spatial extrapolation under scenarios of high variability and limited information in the extreme tail?

2 Methods

2.1 General aspects of the Maximum Certainty Principle

2.1.1 Possible and probable

We begin by conceptually separating the possible and the probable. The possible is a space that requires structure or relational order to be operable and interpretable; without order, one cannot navigate the possible. Without order, the possible is absolute chaos: a set without structure, without relations, without distances, and without utility. Order allows scenarios to be compared and proximity, transition, or evolution to be defined. Thus, the possible is related to a structural geometry. A space without geometry or topology implies that any configuration is possible, whereas a space with geometry implies that some configurations are permitted and others are restricted.

Consider a random experiment ϵ_o: selecting an object with replacement from a set of m objects, labeled according to their size or hierarchy: $n = 1$ for the largest and $n = m$ for the smallest. The space of possible states is $\Omega = \{\omega_1, \omega_2, \dots, \omega_m\}$. The discrete random variable is $X(\omega_n) = n$. An elementary random event is a subset of the sample space Ω such that $A = \{\omega_i\} \subseteq \Omega$. Selecting and observing the object is not merely shapeless chance; the outcome space brings a natural (numerical and relational) order that is operable and comparable.

By contrast, the probable in itself has no ordering along the arrow of time; the probable is only magnitude. Probability is a measure defined on a family $\mathcal{F}$ of subsets of the sample space Ω. Within $\mathcal{F}$ lie all events for which it makes sense to assign probabilities. Probability is a measure that assigns to each measurable event a real number between 0 and 1.

$$P: \mathcal{F} \longrightarrow [0,1]$$

.

According to Kolmogorov's axiomatisation (Kolmogorov, 1950), probability is defined as a non-negative, countably additive measure on a σ-algebra of subsets of a sample space Ω, normalized such that: $P(\Omega) = 1$.

For the random experiment ϵ_0, based on many independent observations, one could assign to X an exponential-type probability distribution $P(X = n)$.

https://doi.org/10.5194/egusphere-2026-1317
Preprint. Discussion started: 8 April 2026

$$P(X = n) = p_n = \frac{e^{-\alpha \cdot \frac{n}{m}}}{\sum_{i=1}^{i=m} e^{-\alpha \cdot \frac{i}{m}}} \qquad 1 \le n \le m$$

Example 1: m = 4 and α = 1.

$p_1 = 0.35,\ p_2 = 0.27,\ p_3 = 0.21,\ p_4 = 0.17,$

In practice, due to its size, it is more likely to select object 1 (35%) and less likely to select the small object (17%). Observe that. $\sum_{n=1}^{m=4} p_n = 1$

The sequence p_n has no temporal ordering per se and does not represent any structure. It is indexed by the value of n, where n extracts a hierarchy from the physical medium under study—in this case, the size of the object.

An intuitive way to relate the probable and the possible is to think that the possible defines the set of paths or states accessible to a system, whereas the probable measures the weight or relative importance of each of those states. The analogy of a unit vector in an abstract space helps to visualise direction (possibilities) and magnitude (probabilities).

2.1.2 Temporal pattern

The set of the m possible elementary events available at the beginning of the process, $\Omega = \{\omega_1, \omega_2, \dots, \omega_m\}$, is the space of possible states, but without time. It is the possible, not the sequential. The symbols ω_n denote the system's elementary events, understood as possible states. These states constitute the basic structure of the possible and do not, by themselves, incorporate either temporal order or probabilistic weight.

By contrast, a temporal pattern is a sequence of events observed over time between two known states. It is a discrete, finite, sequential process without replacement. Let $\mathbf{X} = (X_1, X_2, \dots, X_m)$ be a composite random variable, where each component X_n takes values from the set of possible states $\Omega_{\mathbf{X}}^{(n)}$. X_n represents the state observed at the nth stage of the process. Once the final stage is completed, the composite random event ends, because no states remain available to be selected.

Because X is a composite random variable that describes a temporal pattern, the relevant sample space is not Ω, but the space of complete trajectories defined by the ordered permutations of Ω. The sample space of the temporal pattern is:

$$\Omega_{\mathbf{X}}^{(j)} = \left\{\left(\omega_{i_1}, \dots, \omega_{i_m}\right) \in \Omega^m : \ i_n \neq i_k \ si \ n \neq k\right\}$$
$$1 \le i \le m!, \ \ 1 \le n \le m, 1 \le k \le m, 1 \le j \le m$$

where: Ω^m are all imaginable sequences of length m, including sequences with repeated events.

$\Omega_{\mathbf{X}}^{(j)}$ is the possible structure at step j without repeated events.

The probability of the sequence is defined as a measure on the space of complete trajectories rather than on individual events. Probability does not introduce new states nor modify the space of possibilities. Its function is exclusively to weight subsets of $\Omega_{\mathbf{X}}^{(j)}$. In this sense, probability acts as an external operator on the possible, assigning relative magnitudes to previously defined events. While probability distributes weight over the space of possibilities, it does not reduce that space. All states ω_n remain possible as long as $p_n > 0$. Probability therefore does not eliminate possibilities; it ranks them.

https://doi.org/10.5194/egusphere-2026-1317
Preprint. Discussion started: 8 April 2026

2.1.3 Information

In information theory, the amount of information associated with the occurrence of an event with probability p_n is defined in the discrete setting as:

$$I_n = \ln\left(\frac{1}{p_n}\right) = -\ln(p_n), \quad (1)$$

In the continuous setting, the information associated with an event with probability density $f_T(t)$ is:

$$I_t = \ln\left(\frac{1}{f_T(t)}\right) = -\ln\left(f_T(t)\right), \quad (2)$$

Thus, less probable events generate more information (Shannon, 1948) (if logarithms base 2 are used, the unit of information is the *bit*; if the natural logarithm is used, the unit is the *nat*). This quantity, known as *self-information or surprise*, quantifies how unexpected a result is within a probabilistic model. An event with probability one provides no information, whereas low-probability events yield high information values. Observe that information, like probability p_n, has no temporal order.

The concept of information can be extended from the unexpectedness of an individual event to the unexpectedness of a composite event. Each observation represents knowledge of a partial realisation of the process that eliminates incompatible trajectories and reduces the residual sample space. In the temporal domain, information does not redistribute weight over trajectories; it eliminates trajectories.

If the first observation of X_1 is ω_1, the new space is:

$$\Omega_{\mathbf{X}}^{(2)} = \left\{\omega \in \Omega_{\mathbf{X}}^{(1)} : \omega_1 = \varepsilon_1\right\}$$

This expresses that all trajectories that do not begin with ω_1 disappear. Therefore, probabilities are not reduced; possibilities are eliminated.

2.1.4 Entropy

Shannon entropy H introduced by Shannon (1948) quantifies the average uncertainty associated with a discrete source. For a random experiment with n possible outcomes with probability p_n and information associated with each outcome I_n, entropy is defined as the mathematical expectation of the information $\mathbb{E}[I_n]$:

$$H = \mathbb{E}[I_n] = -\sum_{n=1}^{m} p_n \cdot \ln\left(p_n\right), \quad (3)$$

Entropy H does not depend explicitly on the event order n; it depends only on the values of p_n. Because entropy is independent of order, it can be linked to disorder. For m possible outcomes, there are m! distinct permutations of the summation terms that yield the same value of H. For example, for $m = 3$, the same value is obtained for all 3!=6 possible orderings of the three terms $-p_1 \ln(p_1)$, $-p_2 \ln(p_2)$ and $-p_3 \ln\left(p_3\right)$. There is no preference for the order; all sums produce the same value. Entropy

https://doi.org/10.5194/egusphere-2026-1317
Preprint. Discussion started: 8 April 2026

does not encode temporal ordering and does not represent a sequence of events that appear one after another. All possible arrangements lead to the same result; there is no hierarchy or preference order.

2.1.5 Expected Knowledge Potential

The Expected Knowledge Potential, $\mathbb{E}[C_k]$, is a probability-weighted average of Knowledge C_k that, unlike entropy, depends explicitly on the order k.

$$\mathbb{E}[C_k] = \sum_{n=1}^{m} p_n \cdot C_k, \tag{4}$$

Order is related to time, but it is not limited to it. In the present formulation, the Knowledge term $C(n)$ is kept in a strictly increasing order, which defines the hierarchical structure of the process. The different configurations do not arise from reordering $C(n)$, but from the different ways in which the probabilities p_n are associated with that ordered structure. Accordingly, there are k = m! distinct arrangements in which the m partial values $p_n \cdot C(n)$ may be formed. Maximum certainty is obtained for the arrangement in which the ordered Knowledge structure is paired with the probability distribution in its optimal form. For example, let m = 3:

$$\mathbb{E}[C_1] = \overbrace{p_1 \cdot C(1) + p_2 \cdot C(2) + p_3 \cdot C(3)}^{increasing\ order}$$
$$\mathbb{E}[C_2] = p_1 \cdot C(1) + p_3 \cdot C(2) + p_2 \cdot C(3)$$
$$\mathbb{E}[C_3] = p_2 \cdot C(1) + p_1 \cdot C(2) + p_3 \cdot C(3)$$
$$\mathbb{E}[C_4] = p_2 \cdot C(1) + p_3 \cdot C(2) + p_1 \cdot C(3)$$
$$\mathbb{E}[C_5] = p_3 \cdot C(1) + p_1 \cdot C(2) + p_2 \cdot C(3)$$
$$\mathbb{E}[C_6] = p_3 \cdot C(1) + p_2 \cdot C(2) + p_1 \cdot C(3)$$

2.1.6 Certainty

Certainty is a functional that takes the expectation of the sum of ordered Knowledge and unordered Information. Certainty $\aleph_k$ is the sum of the expected Knowledge of order k and the unordered entropy. It represents an expectation of the specific trajectory k among the $m!$ possible ones: $\aleph_k = \mathbb{E}[C_k] + \mathbb{E}[I_n]$.

$$\aleph_k = \mathbb{E}[C_k + I_n]\,, \tag{5}$$

2.1.7 Maximum certainty

Maximum Certainty $\aleph_{max}$ is the maximum value of Certainty $\aleph_k$. It is obtained by maximising the functional $\aleph_k$ via variational calculus (Beltrán, 2023). In its maximum state, $\aleph_{max}$ becomes an invariant with respect to temporal order that operates on each elementary event of the optimal trajectory.

https://doi.org/10.5194/egusphere-2026-1317
Preprint. Discussion started: 8 April 2026

Entropy has no order; however, within disorder one may observe arrangements that coincide with a chosen direction of order. Such arrangements are not imposed by a law; they are simply among the possible configurations of the system. In the maximum state, the information $C_{max} + I_n$ is invariant and can be taken outside the expectation in Eq. (5).

$$\aleph_{\max} = C_{max} + I_n, \tag{6}$$

Example for the truncated discrete exponential distribution with m outcomes.

$$C(n) = -\alpha \cdot \frac{n}{m}, \tag{7}$$

$$\aleph_{\max} = \sum_{n=1}^{m} p_n(-\alpha \cdot \frac{n}{m}) - \sum_{n=1}^{m} p_n \ln p_n$$

$$\aleph_{\max} = \sum_{n=1}^{m} p_n(-\alpha \cdot \frac{n}{m} - \ln p_n)$$

The expression $-\alpha \cdot \frac{n}{m} - \ln p_n$ is invariant:

$$\aleph_{\max} = (-\alpha \cdot \frac{n}{m} - \ln p_n) \sum_{n=1}^{m} p_n$$

$$\aleph_{\max} = -\alpha \cdot \frac{n}{m} - \ln p_n\,, \tag{8}$$

Table 1. Values of the ordered Knowledge term, information term, and invariant certainty $\aleph_{max}$ for the truncated discrete exponential distribution in Example 1.

n	$C(n)$	$-\ln(p_n)$	$\aleph_{\max}$
1	-0.25	1.05	0.80
2	-0.50	1.30	0.80
3	-0.75	1.55	0.80
4	-1.00	1.80	0.80

2.1.8 Maximum Certainty Principle in a continuous field

Whereas in classical inference approaches the functional in the continuous setting is defined on the density function $f_T(t)$ as the primary variable (Cover and Thomas, 2006, p. 409), PCM formulates the problem on the cumulative distribution function $P_T(t)$ with boundary points (0, 0) and (DT, 1). This introduces a genuine variational structure in which the Euler–Lagrange equation takes the form of a conservation law associated with informational invariance with respect to $P_T(t)$. PCM starts from $\aleph_{\max}$ and obtains the density function $f_T(t)$ as a function of the available Knowledge $C(t)$ with $0 \le t \le DT$:

$$\aleph_{\max} = \mathrm{C(t)} - \underbrace{\ln(f_{T_C})}_{surprise}\,, \tag{9}$$

https://doi.org/10.5194/egusphere-2026-1317
Preprint. Discussion started: 8 April 2026

$$f_T(t) = \frac{e^{C(t)}}{\int_0^{DT} e^{C(t)} dt}, \tag{10}$$

The denominator is known as the partition function:

$$Z = \int_0^{DT} e^{C(t)} dt, \tag{11}$$

$$\aleph_{max} = ln \int_0^{DT} e^{C(t)} dt = \ln(Z), \tag{12}$$

The Knowledge Potential $C(t)$ is characterized as the sum of monotonic functions. Experience $E(t)$ is decreasing, and $Cr(t)$ is increasing or constant. In the example of Fig. 1: $E(t) = -\lambda t - \aleph_{max}$ and $Cr(t) = 0$. Variations of the functions $E(t)$ and $Cr(t)$ generate the different probability distributions used in inferential statistics.

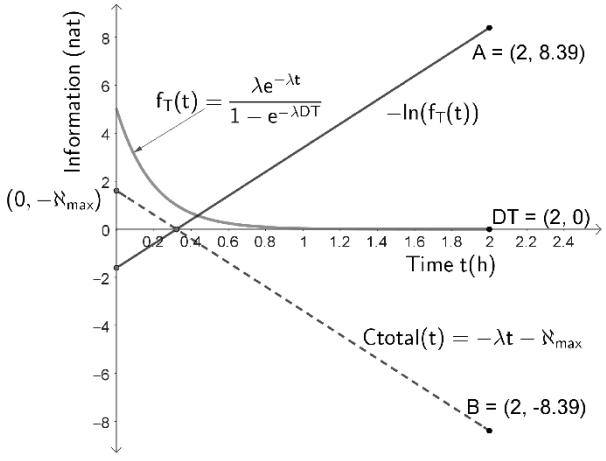

Figure 1. Information associated with the truncated exponential distribution function for $DT = 2\ h, \lambda = 5\ h^{-1}$.

Classical probabilistic inference approaches, such as the Maximum Entropy Principle (MEP), select a distribution compatible with a given set of constraints. In this framework, the outcome is a density that satisfies specific statistical conditions, but the procedure does not explicitly introduce a structure over the space of possible trajectories.

In contrast, PCM defines a functional over the space of possibilities through the interaction between a Knowledge Potential and an informational term. The extremal condition not only determines an optimal density but also induces a hierarchical organisation of trajectories: the path that maximises the functional can be interpreted as structurally privileged, whereas other configurations remain as possible paths, albeit with lower probabilistic weight.

This difference is relevant in systems where the temporal sequence of events has physical or interpretative meaning, as in the case for storm events. In such contexts, it is not only the probability distribution of intensities or precipitation that matters, but also the internal structure of the event and its possible alternative configurations. PCM makes it possible to preserve this multiplicity of trajectories within a framework ordered by the functional, rather than reducing the analysis to the selection of a single distribution compatible with aggregated constraints.

https://doi.org/10.5194/egusphere-2026-1317
Preprint. Discussion started: 8 April 2026

2.2 Applications to dissipative phenomena

The developments presented in the previous sections establish PCM as a general framework for selecting distributions and trajectories compatible with a set of structural and informational constraints. In particular, it has been shown that certainty is not identified with a high probability of isolated events, but with the progressive organisation of the space of possible trajectories through the coexistence of entropy and structural order. This approach is especially pertinent in dissipative systems, in which temporal evolution is not adequately described by instantaneous states, but rather by complete trajectories defined over finite time intervals. In such systems, the dissipation of energy, mass, or information introduces temporal directionality and favours the emergence of patterns that structure the observed dynamics.

The distinctive contribution of PCM is not only that it yields a truncated exponential representation, but that it formulates temporal evolution as an optimal trajectory within a family of admissible paths between the initial and final states. In this framework, the optimal path is associated with an invariant quantity that provides a structural interpretation of the process. This offers a basis for going beyond empirical curve fitting and for interpreting dissipative phenomena in terms of event structure and temporal organisation.

Convective storms are a paradigmatic example of this type of process. A pluviograph can be interpreted as a temporal trajectory of accumulated precipitation, defined over a finite duration $DT(h)$, whose shape reflects dissipative mechanisms associated with the progressive release of energy and moisture. From this perspective, storm modelling is not reduced to estimating marginal distributions, but requires identifying typical temporal patterns that organize precipitation discharge in time.

Similarly, nonequilibrium geomorphological processes, such as the progressive recovery of river channels subjected to severe disturbances, can be understood as possible dissipative trajectories over a finite time interval DT. A recent example is provided by the Coca River (Ecuador), where a sudden geomorphic disturbance initiated a clearly time-bounded adjustment trajectory. After the collapse of the San Rafael waterfall in February 2020 on the Coca River, an abrupt knickpoint developed, triggering a regressive erosion process with rapid retreat of the erosional front in the months following the collapse and an exceptional sediment pulse (Barrera-Crespo et al., 2024). Numerical modeling of waterfalls with a resistant cap layer shows that retreat rate can vary over time and depend not only on hydraulic energy, but also on the resistance of the underlying formation and downstream incision conditions (Haviv et al., 2010). After an abrupt perturbation of the longitudinal profile, the system may exhibit an initial phase dominated by mechanical failures and high gradient, followed by a progressive adjustment controlled by downstream incision dynamics. In this context, the temporal evolution of the system can be interpreted as the dynamics of a complex system resulting from the interaction between energy dissipation and structural reconfiguration, a process that can be conceived as a progressive selection of geomorphological trajectories within a space of possible configurations.

In the following section, this interpretation is adopted and it is shown how PCM can be used to identify structurally privileged temporal patterns in dissipative systems. In particular, a truncated exponential functional is introduced to represent pluviographs as optimal temporal trajectories over a finite interval DT, establishing an operational link between PC and

https://doi.org/10.5194/egusphere-2026-1317
Preprint. Discussion started: 8 April 2026

physical parameters of the phenomenon. This approach lays the groundwork for using PCM in rainfall simulation and regionalisation.

2.3 Rainfall modelling in the DMQ

Storms in the Metropolitan District of Quito (DMQ) have been simulated using the Storm Information Model for Quito (MIT-Q). Initially, this model was designed to simulate the spatiotemporal representation of precipitation over 1600 km², based on 289 daily pluviographs of intense storms spanning 73 years (1916–1992) at the Quito-Observatory station. In a 200-year stochastic simulation, maximum rainfall intensities ($mm.h^{-1}$) for durations between 10 min and 6 h were extracted and compared, using an error criterion, with the official IDF curves of the Metropolitan Public Water and Sanitation Company of Quito (EPMAPS) (Empresa Metropolitana de Alcantarillado y Agua Potable [EMAAP-Q], 2009), thereby allowing the model parameters to be calibrated (Beltrán, 2021). A demonstration video of the MIT-Q model is available online (Beltrán, 2024). For the present study, the study area is 2500 km² and calibration and validation are performed through 500-year stochastic modelling. MIT-Q uses physically meaningful variables and parameters, such as storm duration $DT(h)$, modelled with the truncated exponential distribution; accumulated precipitation PRE (mm), modelled with the Weibull distribution, and the number of rainfall bursts α. MIT-Q simulates the effects of storm cells advected by local winds driven by the gradient of annual isohyetals in the DMQ. The model provides synthetic statistical data that, through parameter-sensitivity techniques, can be calibrated and validated against official information.

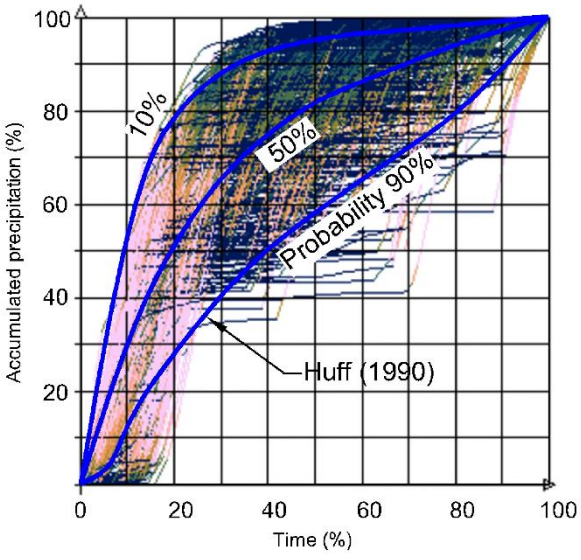

Figure 2. Time distribution of first-quartile storms according to Huff (1990) and of 475 first-quartile storms (Pre ≥ 15 mm) simulated with MIT-Q.

The temporal evolution of a storm can be segmented into three stages: initiation, development, and dissipation. In the initial stage, the cloud begins to produce rainfall at low intensity. During development, the storm reaches its maximum intensity and

https://doi.org/10.5194/egusphere-2026-1317
Preprint. Discussion started: 8 April 2026

precipitates most of its total volume. Finally, in the dissipation stage, intensity decreases until it progressively ceases. Huff (1990) summarised storm temporal patterns according to whether the largest fraction of total rainfall occurs in the first, second, third, or last quarter of the event, indicating that intense storms frequently exhibit early-peaked behaviour (Fig. 2).

The quartile-based time-distribution framework has also been applied in other settings. For example, Back (2011) reported that, in Urussanga (Brazil), type I storms were the most frequent (42.4%), followed by type II storms (31.1%), illustrating the broader applicability of quartile-based temporal patterns for describing intra-event structure. In the methodology adopted here, PCM and MIT-Q provide an operational basis for representing this intra-event structure through a truncated exponential formulation.

2.3.1 MIT-Q fundamentals

The recurrence frequency of various natural phenomena can be represented by an exponential random variable. Examples include the time between seismic events of a given magnitude in a region, radioactive decay, and the lifetime of electronic components and the time to the next failure in mechanical systems.

A truncated exponential distribution limits the random variable to a maximum value DT. Its usefulness is evident in the statistical representation of intense events, or their impacts, such as landslides during earthquakes (Kiran et al., 2016), or in the distribution of extreme-rainfall cluster sizes worldwide (Traxl et al., 2016), and studies of magnitude–frequency relationships in earthquake statistics (Cosentino et al., 1977).

Storm time can be represented by a truncated exponential random variable. The continuous random variable T (h) represents the residence time in the development state, or the ability to remain in optimal conditions until reaching an unsustainable point. The probability of remaining in optimal development for a time T less than or equal to $t(h)$, truncated at $DT(h)$ and with rate $\lambda_0 = \frac{\alpha_0}{DT}$, is computed as:

$$P_{\lambda_0 T}(t) = P_{\lambda_0}(T \leq t | T \leq DT) = \frac{1-e^{-\lambda_0 \cdot t}}{1-e^{-\lambda_0 \cdot DT}}, \quad (13)$$

MIT-Q applied to storms in the DMQ yielded a storm functional whose optimal temporal pattern, expressed by Eq. (13) and squared, is proportional to the accumulated precipitation Pre(t) (mm), normalized by the maximum precipitation PRE (mm).

$$\frac{Pre(t)}{PRE} \cong \left(P_{\lambda_0 T}(t)\right)^2, \quad (14)$$

The squared form was adopted empirically because it provided the most consistent representation of the normalised accumulated precipitation within MIT-Q. In particular, whereas the truncated exponential distribution itself is strictly decreasing, its squared cumulative form reproduces a more realistic storm evolution, including an initial growth stage followed by development and subsequent dissipation.

Equation (13) is substituted into Eq. (14).

https://doi.org/10.5194/egusphere-2026-1317
Preprint. Discussion started: 8 April 2026

$$Pre(t) = PRE\left(\frac{1-e^{-\lambda_0 t}}{1-e^{-\lambda_0 DT}}\right)^2, \quad (15)$$

With respect to dissipative dynamics, MIT-Q represents the system from an information-based perspective. The system transitions from the initial state, called the Lambda state ($\lambda_0 = \lambda$, $C_\lambda(t) = -\lambda t$, to the final state ($\lambda_0 = 0, C_0(t) = 0$) over a time interval $t_d(h)$, called the development time.

$$\aleph max_\lambda = -\lambda t - \ln(f_{\lambda_T}) = -\ln\left(\frac{\lambda}{1-e^{-\lambda DT}}\right)$$

$$\aleph max_0 = 0 - \ln(f_{0_T}) = -\ln\left(\frac{1}{DT}\right)$$

$$\Delta\aleph max = \aleph max_0 - \aleph max_\lambda = \ln\left(\frac{\lambda DT}{1-e^{-\lambda DT}}\right)$$

$$t_d = \frac{\Delta\aleph \max}{\Delta C(t)'} = \frac{\aleph max_0 - \aleph max_\lambda}{C_0'(t) - C_\lambda'(t)} = \frac{\ln\left(\frac{\lambda DT}{1-e^{-\lambda DT}}\right)}{0-\lambda}, \quad (16)$$

$$t_d = \frac{DT}{\alpha_0}\ln\left(\frac{\alpha_0}{1-e^{-\alpha_0}}\right), \quad (17)$$

The development stage ends at $T = t_d$, after which the event decays. The set of possible trajectories is not reduced from $\lambda_0 = \lambda$ to $\lambda_0 = 0$. However, in state $\lambda_0 = 0$, one trajectory cannot be distinguished from another.

For computational modelling, the mean temporal pattern between the two states is used:

$$\bar{P}_{\lambda o_T}(t) = \frac{1}{2}\left(\frac{1-e^{-\lambda o \cdot t}}{1-e^{-\lambda o \cdot DT}} + \frac{t}{DT}\right), \quad (18)$$

The rate $\lambda_0 = \frac{\alpha_0}{DT}$ simulates the complex effects of the formative dynamics of precipitable water droplets reaching the surface. It represents the repeated expansive attempts to develop into storm cells until gravity suppresses these upward pulses. After this contest, large masses of water precipitate to the surface. Observe that λ_0 does not include wind-advection effects.

https://doi.org/10.5194/egusphere-2026-1317
Preprint. Discussion started: 8 April 2026

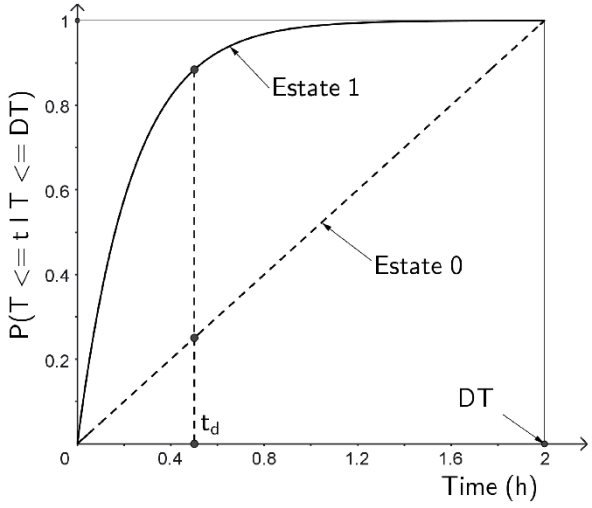

Figure 3. Conceptual state transition of storm development in MIT-Q, from the initial Lambda state to the final state over the development time interval DT.

2.3.2 Winds and temporal patterns in MIT-Q

Recorded pluviographs are subject to factors such as local wind direction and speed, which influence the amount and temporal pattern of precipitation reported by instruments. Local winds spread rainfall over large areas, decreasing mean intensity on the leeward side and increasing it on the windward side. Areas where intensities are high are typically highly concentrated (Fig. 4a) and may be missed by a low-density network of meteorological stations. The optimal temporal pattern with rate λ_0 from Eq. (15), when advected by local spatial motions, shifts towards a distorted pattern with rate λ_v. As an example, a particular synthetic storm modelled with MIT-Q (DT = 7.8 h, PRE = 58.4 mm, $\alpha_0 = 10$, mean precipitation 22.6 mm, minimum precipitation 10.0 mm) produced α_v values between 2.4 and 14.6 with mean α_v= 8.6 (Fig. 4b). Temporal patterns in the zone of high intensities (C) tend towards high α_v values, whereas in zone A the $\alpha_v$values are moderate (6.5─8.0).

A synthetic sample of 475 first-quartile storms with PRE > 15 mm at the virtual Quito-Observatory station over 50 years of modeling yielded $\alpha_v$values between 15.2 and 5.1 with mean α_v= 8.6, as shown in Fig. 2. The curve from Eq. (15) that best fits Huff's first-quartile 10% curve is obtained with α_v= 12.7. The value α_v= 5.8 provides the best fit to the 50% curve, and α_v= 2.8 to the 90% probability curve.

Winds distribute precipitation depth over large areas. On the windward side, they help concentrate and increase rainfall intensities over small areas.

The mean intensity of a specific storm advected by winds is obtained by dividing Eq. (15) by duration t, substituting λ_v for λ_o and $\lambda_v = \frac{\alpha_v}{DT}$.

$$\bar{I}(t) = \frac{PRE}{t} \cdot \left(\frac{1-e^{-\alpha_v \frac{t}{DT}}}{1-e^{-\alpha_v}} \right)^2, \quad (19)$$

https://doi.org/10.5194/egusphere-2026-1317
Preprint. Discussion started: 8 April 2026

The instantaneous rainfall intensity I(t) (mm.h^{-1}) of a specific wind-advected storm is obtained by differentiating Eq. (15) with respect to time:

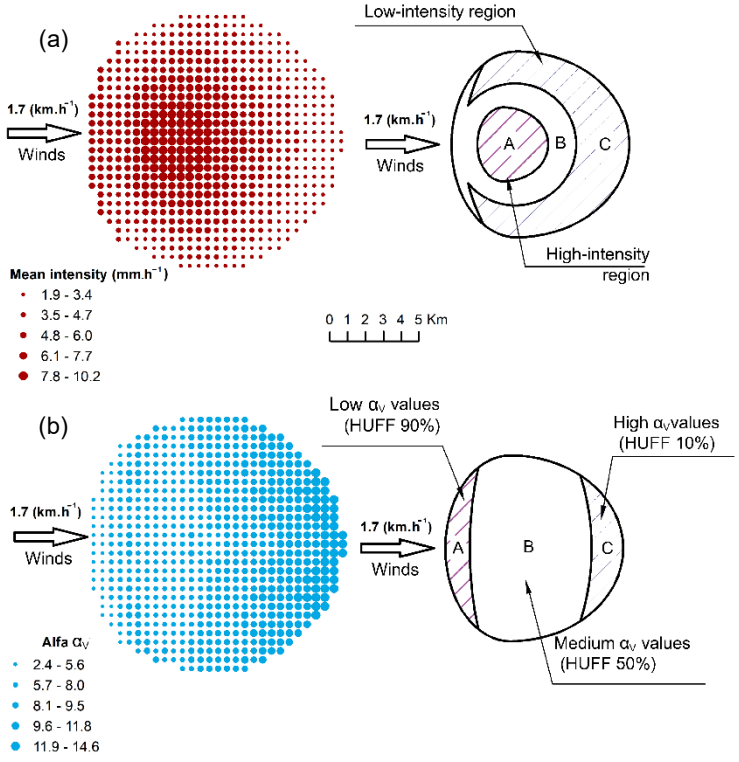

Figure 4. (a) Mean rainfall intensities within a synthetic storm simulated with MIT-Q. (b) Spatial distribution of α_v values for the same synthetic storm.

$$I(t) = 2PRE\frac{\alpha_v}{DT}\frac{\left(1-e^{-\alpha_v\cdot\frac{t}{DT}}\right)e^{-\alpha_v\cdot\frac{t}{DT}}}{(1-e^{-\alpha_v})^2} \quad , \tag{20}$$

2.3.3 MIT-Q calibration and validation

From a 500-year stochastic simulation, maximum rainfall intensities for durations between 5 min and 12 h were extracted and compared, using an error criterion, with the official EPMAPS IDF curves to calibrate the model parameters. Temporal patterns of individual events exhibited truncated-exponential behaviour in DT, with parameter $\alpha_0 = \lambda_0 \cdot \mathrm{DT}$, where α_0 was calibrated to 10 using data from the century-old M-054 Quito-Observatory meteorological station (0° 12′ 53.7″ S, 78° 30′ 9.3″ W). Here, α_0 is the number of rainfall bursts in development within duration DT. The model fit during the calibration stage is shown in Fig. 5a. Next, the simulated intensities were compared with those at other stations to validate MIT-Q: M-003 Izobamba (0° 21′ 58″ S, 78° 33′ 19″ W), M-024 Iñaquito (0° 10′ 40″ S, 78° 29′ 15″ W), M-002 Tola (0° 13′ 43″ S, 78° 22′ 2″ W), and P10 DAC-Aeropuerto (0° 8′ 43″ S, 78° 29′ 13″ W). Validation at the four additional meteorological stations is shown in Figs. 5b–

https://doi.org/10.5194/egusphere-2026-1317
Preprint. Discussion started: 8 April 2026

e. Validation of the Iñaquito station is carried out against the study by Escobar et al. (2022), station P09 Iñaquito. The Aeropuerto station is validated against the study by Palacios et al. (2015), station P10 DAC-Aeropuerto.

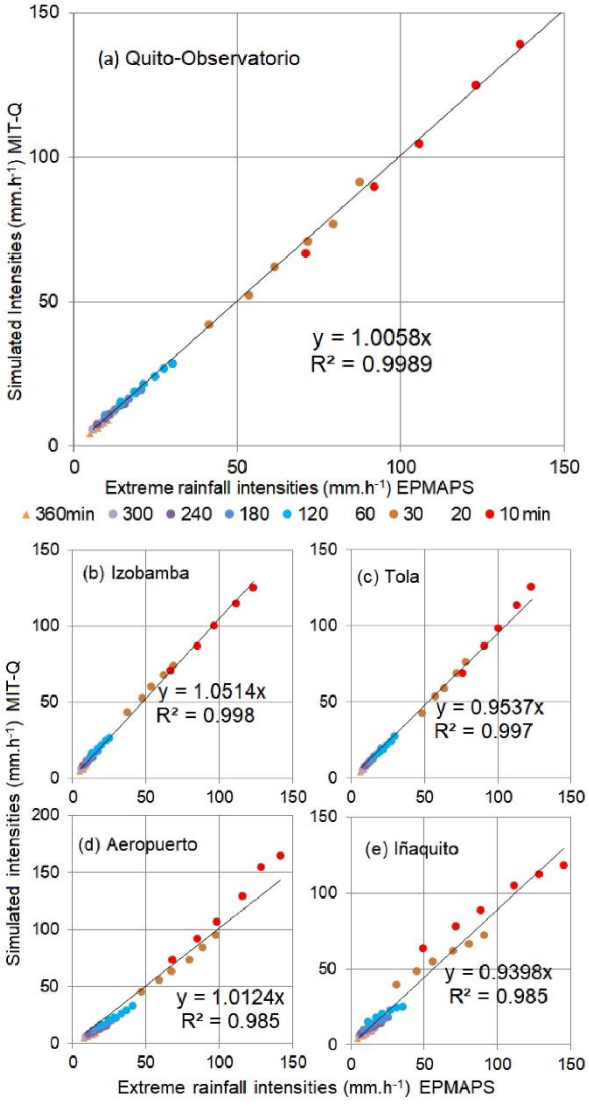

Figure 5. Calibration and validation of MIT-Q against observed IDF curves. (a) Calibration at the Quito-Observatory station. Validation at (b) M-003 Izobamba; (c) M-002 Tola; (d) P10 DAC Aeropuerto, and (e) P09 Iñaquito. Station locations are shown in Fig. 6.

2.3.4 MIT-Q thematic maps

Several thematic maps can be extracted from MIT-Q modelling. For example, Fig. 6a shows the number of rainfall events per year with precipitation greater than 0.1 mm. Extreme rainfall intensities for a 50-year return period and 1 h duration are shown

https://doi.org/10.5194/egusphere-2026-1317
Preprint. Discussion started: 8 April 2026

in Fig. 6b. Although these values vary markedly among neighbourhoods, they are amenable to regionalisation. The batlow colour map of Crameri et al. (2020) was used; its perceptually uniform gradation improves the readability of spatial patterns and allows a clearer interpretation of the mapped classes. The gentle slopes of the Quito basin, flanked by the Guagua Pichincha volcano, the Atacazo hill, and the Puengasí hill, show low intensities with high spatial homogeneity, but also zones of high intensities on steep topographic slopes.

Evidence of the extreme spatial heterogeneity of downpour intensities is that, despite a dense network of meteorological stations installed in the Quito basin (18 rain gauges and pluviographs), a particularly devastating flood in the La Raya gully went unnoticed in the pluviometric records (Pourrut, 1995).

This is not an isolated case: the debris flow in the Miraflores ravine in the La Gasca area on 25 February 1975 was not recorded as one of the four relevant storms at the Quito-Observatory station in 1975. Press records of 317 accident events following storms were compiled by Pourrut and Leiva (1989) from 1900 to 1988. A search of the Quito-Observatory meteorological station records by accident dates yielded 26 storms, of which 16 had durations shorter than 2.1 h and mean precipitation of 31.3 mm. Their mean intensities corresponded to return periods averaging only 5 years. This provides evidence that most of the precipitation that caused damage in surrounding neighborhoods escaped detection at this century-old station (Beltrán, 2017). Given the high areal concentration of rainfall intensities, the station network should be dense to identify them. In sparse networks, intensities should be adjusted upwards to represent potential point storm intensities.

In hydrology, mean intensities over a drainage basin are computed as the product of the maximum point rainfall intensity and a reduction coefficient. If the maximum point rainfall intensity is underestimated because it was not captured by a sparse pluviograph network, basin-average estimates may be biased low. The answer suggests that, in sparse networks such as those in Ecuador, additional safety factors should be considered to represent potential point storm precipitation.

Another important conclusion from the modelling is the substantial decrease in the correlation ($R^2 \leq 0.64$) between maximum short-duration rainfall intensities (duration $\leq$ 2.0 h) and daily rainfall intensity (duration = 24 h). This means that, for regionalisation, using daily intensity to obtain intensities shorter than 2 h is not advisable in the DMQ.

This result supports the structural separation between maximum event precipitation (PRE) and event duration (DT) adopted in MIT-Q. Since the functional is defined over the storm interval ending at DT, the relevant temporal scale of the process is the event duration rather than a fixed 24 h period. For short-duration storms, PRE/DT is therefore more representative than PRE/24 h, whereas daily intensity becomes more informative only for longer-duration events.

https://doi.org/10.5194/egusphere-2026-1317
Preprint. Discussion started: 8 April 2026

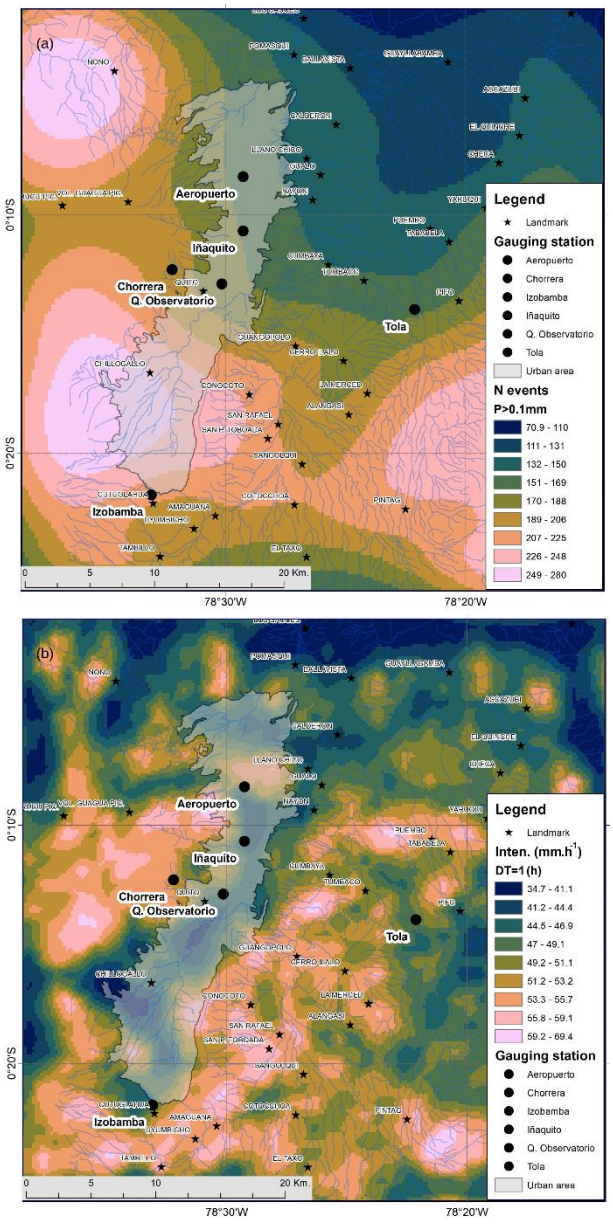

Figure 6. Thematic maps derived from MIT-Q. (a) Number of rainfall events per year with precipitation greater than 0.1 mm. (b) Rainfall intensity (mm h−1) for a return period of 50 years and a duration of 1 h.

2.4 Regionalisation of Intensity–Duration–Frequency curves in Ecuador

The transfer from the DMQ to the national INAMHI framework does not assume that the calibrated local parameter values from Quito are valid throughout Ecuador. What is transferred is the conceptual and methodological structure developed with MIT-Q, namely the representation of storm development through an optimal temporal pattern, its associated invariant, and the

https://doi.org/10.5194/egusphere-2026-1317
Preprint. Discussion started: 8 April 2026

corresponding interpretation of extreme-event structure. This framework is then applied station by station using the local INAMHI IDF information available at each site.

The National Institute of Meteorology and Hydrology of Ecuador (INAMHI) published two IDF curves for each of the 66 pluviograph stations, corresponding to short- and long-duration ranges, of the form:

$$\bar{I}_{Tr}(t) = \frac{a \cdot ID_{Tr}}{60^b \cdot t^b}, \tag{21}$$

where a and b are station-specific fitting constants, and ID_{Tr} is the daily intensity (mm.h^{-1}) for a return period Tr (years). For unit consistency, duration t is expressed in hours.

The instantaneous intensity $I_{Tr}(t)$ of the INAMHI curves is obtained by multiplying Eq. (21) by duration t and then differentiating with respect to time:

$$I_{Tr}(t) = \frac{a \cdot (1-b) \cdot ID_{Tr}}{60^b \cdot t^b}, \tag{22}$$

2.4.1 Extreme storm for each point on the INAMHI IDF curves

To transform a storm with parameters:(PRE, DT) into an extreme storm (PRE_{Tr}, DT), it is required that the storm mean-intensity curve (Eq. (19)) and the INAMHI IDF curve (Eq. (21)) share a common tangency point. Both equations are set equal and (PRE_{Tr}, DT) is solved for:

$$PRE_{Tr} = \frac{a \cdot ID_{Tr}}{t^{b-1} \cdot 60^b} \cdot \left(\frac{1-e^{-\alpha_v}}{1-e^{-\tau}}\right)^2, \tag{23}$$

where:

$$\tau = \alpha_v \cdot \frac{t}{DT}, \tag{24}$$

To achieve tangency, the instantaneous intensity equations, Eq. (20) and Eq. (22), are set equal, and PRE_{Tr} from Eq. (23) is substituted.

$$\frac{2\tau e^{-\tau}}{1-e^{-2\tau}} = 1 - b\,, \tag{25}$$

τ is constant over the range of durations under study and can be computed iteratively. τ is obtained by solving Eq. (17) for τ using the ratio $\alpha_o \frac{t_d}{DT}$.

$$\tau = \alpha_o \frac{t_d}{DT} = \ln\left(\frac{\alpha_o}{1-e^{-\alpha_o}}\right), \tag{26}$$

Because τ is obtained experimentally from b in Eq. (25), the measured storm events are influenced by wind drag and, therefore, the α_o resulting is α_v.

$$\Delta\aleph\max = \tau = \alpha_v \frac{t_d}{DT} = ln\left(\frac{\alpha_v}{1-e^{-\alpha_v}}\right), \tag{27}$$

https://doi.org/10.5194/egusphere-2026-1317
Preprint. Discussion started: 8 April 2026

With this approach, the INAMHI coefficient b is transformed into the potential number of rainfall bursts within DT affected by wind drag α_v , giving it physical meaning. At the same time, α_v defines the most recurrent storm temporal pattern. These elements had previously been disconnected.

Given τ and α_v, the duration DT of an individual storm associated with an intensity of duration t_d is obtained from Eq. (27) as:

$$DT = \frac{\alpha_v t_d}{\tau}, \tag{28}$$

The precipitation PRE_{Tr} over DT of an individual storm associated with an intensity of duration t_d is:

$$PRE_{Tr} = \frac{\bar{I}_{Tr}(t_d)\cdot t_d}{\left(\frac{1-e^{-\tau}}{1-e^{-\alpha_v}}\right)^2}, \tag{29}$$

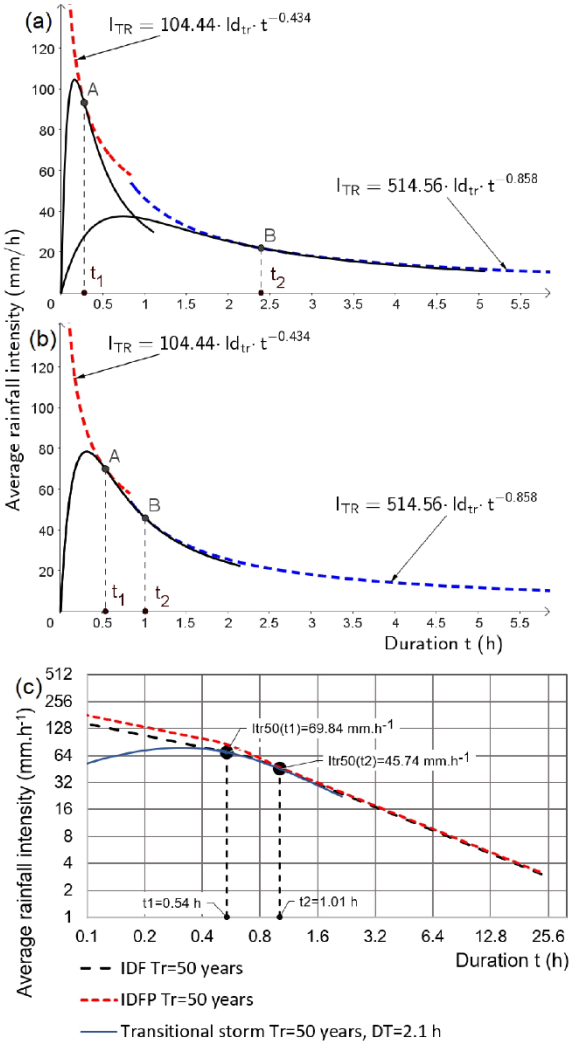

https://doi.org/10.5194/egusphere-2026-1317
Preprint. Discussion started: 8 April 2026

Figure 7. INAMHI IDF curves for station M003-Izobamba (Tr = 50 years). (a) Two extreme storms obtained from Eq. (19): a short-duration storm (DT = 1.1 h, PRE = 32.9 mm, α_v = 8.6), tangent to the INAMHI IDF curve at t = 0.28 h, and a long-duration storm (DT = 5.06 h, PRE = 54.2 mm), tangent at t = 2.39 h. (b) Transition storm (DT = 2.15 h, PRE = 48.0 mm, α_v = 8.6), tangent at t = 0.53 h and t = 1.01 h. (c) IDFP curves for station M003-Izobamba (Tr = 50 years).

Each duration point t on the INAMHI IDF curves can now be represented by a corresponding duration point t_d of a particular extreme storm with maximum precipitation PRE_{Tr} and storm duration DT. For example, Fig. 7a shows two extreme storms at the Izobamba meteorological station, one associated with short durations and the other with long durations.

2.4.2 Transition storm

To obtain a particular storm function located at the boundary between short and long durations, the concept of a transition storm is introduced. The transition storm is tangent to both the short-duration IDF curve and to the long-duration IDF curve. The transition storm is not introduced here as an independently fitted empirical object. Rather, it follows from the consistent application of the quadratic storm function to the short- and long-duration INAMHI IDF regimes, under the requirement that a single storm function be tangent to both.

As a single storm defined over the tangency interval, it satisfies $DT_1 = DT_2$ and $\alpha_{v1} = \alpha_{v2}$, which implies the following relationship:

$$\frac{\tau_1}{\tau_2} = \frac{\alpha_{v1}\frac{t_1}{DT_1}}{\alpha_{v2}\frac{t_2}{DT_2}} = \frac{t_1}{t_2}$$

$$t_1 = t_2\frac{\tau_1}{\tau_2}\,, \tag{30}$$

where: t_1 is the start time of the transition segment.

t_2 is the end time of the transition segment.

τ_1 comes from Eq. (26) for the low-duration range, and τ_2 for the high-duration range.

In the range t_1 to t_2 of the transition storm, the following also holds:

$$PRE_{Tr_1} = PRE_{Tr_2}\,, \tag{31}$$

Equations (23) and (30) are substituted into Eq. (31), and t_2 is solved for:

$$PRE_{Tr} = \frac{\bar{I}_{\mathrm{Tr}}(t_d)\cdot t_d}{\left(\frac{1-e^{-\tau}}{1-e^{-\alpha_v}}\right)^2}\,, \tag{32}$$

Equations (30) and (32) allow the transition interval between t_1 and t_2 to be computed for the storm transition function. This approach unifies short- and long-duration characteristics within the $t_1 - t_2$ interval into an envelope curve that captures the dynamics of both ranges (Fig. 7b).

https://doi.org/10.5194/egusphere-2026-1317
Preprint. Discussion started: 8 April 2026

3 Results

3.1 Potential IDF curves (IDFP)

The invariant is not treated here merely as an internal quantity of the variational formulation, but as the structural quantity that links each empirical IDF point to a corresponding extreme storm-development state. This is what allows the observed IDF behaviour to be reinterpreted in terms of storm structure and, subsequently, to derive IDFP curves under sparse station coverage.

The potential rainfall intensity $\bar{I}_p(t)$ is the INAMHI rainfall intensity, $\bar{I}_{Tr}(t)$; in which the value of α_{v1} is increased up to α_{v2}. This expresses that, potentially, for any interval, $\frac{t_1}{DT_1}$ and $\frac{t_2}{DT_2}$ are equal and α_{v1} can reach the value of α_{v2}.

$$\frac{\tau_1}{\tau_2} = \frac{\alpha_{v1}\frac{t_1}{DT_1}}{\alpha_{v2}\frac{t_2}{DT_2}} = \frac{\alpha_{v1}}{\alpha_{v2}}$$

$$\alpha_p = \alpha_{v2} = \alpha_{v1} \cdot \frac{\tau_2}{\tau_1}, \tag{33}$$

$$\bar{I}_p(t) = \bar{I}_{Tr}(t) \cdot \frac{\left(\frac{1-e^{-\alpha_p \cdot \frac{t}{DT}}}{1-e^{-\alpha_p}}\right)^2}{\left(\frac{1-e^{-\alpha_v \cdot \frac{t}{DT}}}{1-e^{-\alpha_v}}\right)^2}, \tag{34}$$

The intensity scaling factor is defined as:

$$\varphi = \frac{\left(\frac{1-e^{-\alpha_p \frac{t}{DT}}}{1-e^{-\alpha_p}}\right)^2}{\left(\frac{1-e^{-\alpha_v \frac{t}{DT}}}{1-e^{-\alpha_v}}\right)^2}, \tag{35}$$

The potential storm intensity is the INAMHI intensity affected by a scaling factor φ.

$$\bar{I}_p(t) = \bar{I}_{Tr}(t) \cdot \varphi, \tag{36}$$

Figure 7c illustrates the application at station M003-Izobamba, where $\varphi = 1.24$ for short-duration storms and $\varphi = 1.03$ for long-duration storms.

The methodology is replicable across the 66 INAMHI stations throughout Ecuador. The $\varphi - b$ relationship shows a strong correlation for both short and long durations (Fig. 8a).

$$\varphi(b) = b^{-0.237}, \tag{37}$$

IDFP curves are equivalent to multiplying the INAMHI IDF curves by a single function over the entire range of durations, equivalent to a scaling factor:

https://doi.org/10.5194/egusphere-2026-1317
Preprint. Discussion started: 8 April 2026

$$\overline{I_p}(t) = \frac{a \cdot ID_{Tr}}{60^{b} \cdot t^{b}} \cdot \varphi(b), \quad (38)$$

Figure 8b compares rainfall bursts values at the regional scale and at the local scale (DMQ). The potential α_v values at station M054 Quito Observatorio reach a maximum of $\alpha_v = 35.6$, indicating the capacity for strong early storm development. Across the INAMHI stations, a maximum of $\alpha_p = 24.9$ is obtained.

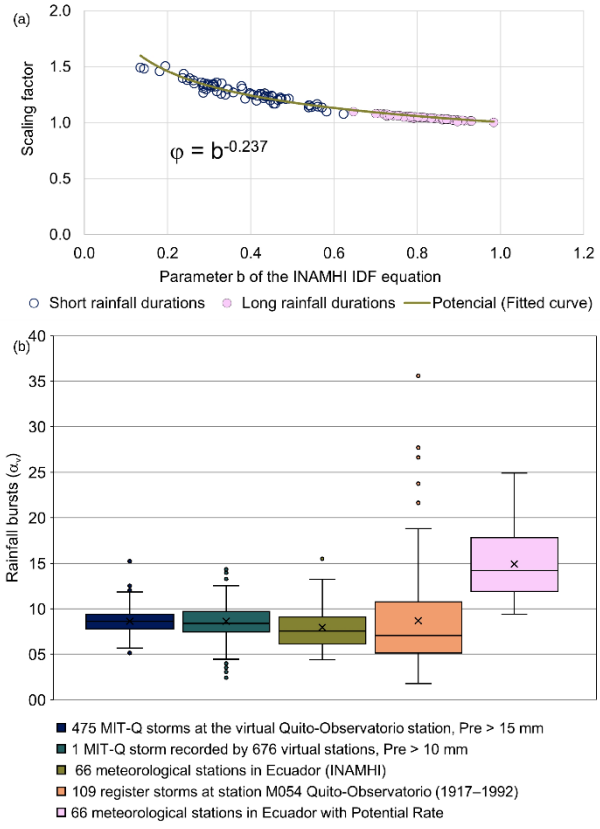

Figure 8. (a) Relationship between the INAMHI parameter b and the scaling factor; (b) Comparison of α_v values (number of rainfall bursts) at the regional scale and in the DMQ.

The maps in Fig. 9 show the scaling factor for INAMHI official extreme intensities, for both short and long durations. The maximum change is observed at station M073 Taura-Aeropuerto, where, for example, 10 min rainfall intensities increase from 185 mm.h^{-1} to 279 mm.h^{-1} for a 25-year return period. Potential intensities correspond to the storm activity centre and should be interpreted as point maximum intensities. To obtain areal-average intensities over the storm coverage area, reduction coefficients should be applied due to the increase in wetted area.

From a regional perspective, intensities increase by 8% to 51% for short durations and by up to 10% for long durations, mainly along the coastal zone and at the foothills of the western and eastern cordilleras. Within the inter-Andean valley, an average increase of 24 % is observed for short-duration intensities, compared with 3% for long-duration intensities.

https://doi.org/10.5194/egusphere-2026-1317
Preprint. Discussion started: 8 April 2026

500

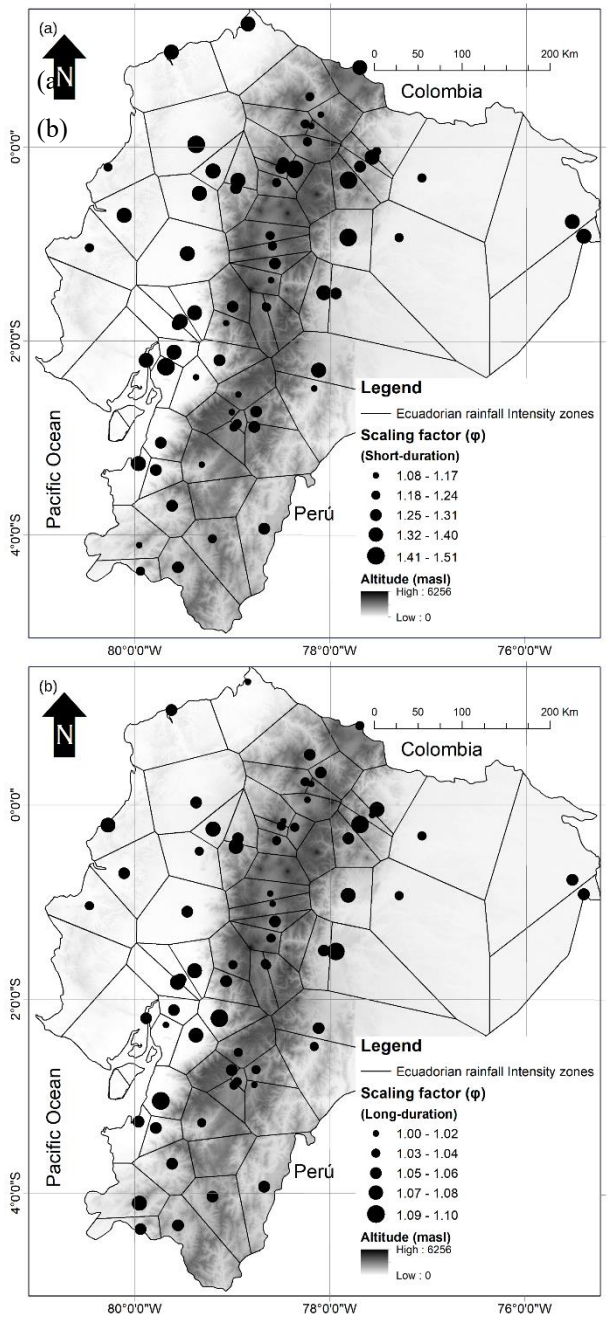

Figure 9. Regionalisation of the scaling factor applied to Ecuador rainfall intensities: (a) short durations and (b) long durations. Hillshade derived from ASTER GDEM V3 (ASTGTM.003) (NASA/METI/AIST/Japan Spacesystems and U.S./Japan ASTER Science Team, 2019).

505

https://doi.org/10.5194/egusphere-2026-1317
Preprint. Discussion started: 8 April 2026

4 Conclusions

This study introduces and applies the Maximum Certainty Principle (PCM) as a variational framework for probabilistic modelling and provides adjustments to the existing national regionalisation of extreme rainfall in Ecuador. Formulating PCM with respect to the cumulative distribution function, with explicit boundary conditions, allows the temporal evolution of storms to be interpreted as an optimal trajectory within a structured space of admissible configurations.

On the applied side, the MIT-Q model shows that a truncated exponential representation of intra-event structure can coherently reproduce Intensity–Duration–Frequency curves through long-term stochastic simulations. Validation at four additional stations suggests that the explicit separation between maximum event precipitation (PRE) and event duration (DT) constitutes a relevant conceptual advance over approaches that use daily intensity as a representative variable, particularly for short-duration storms. An operational contribution of this work is the introduction of Potential IDF (IDFP) curves and the scaling factor $\varphi(b)$, which enable a structural reinterpretation of the empirical parameter b used in national formulations. This extension provides a practical way to adjust extreme rainfall estimates when station coverage is sparse.

Although PCM can recover exponential-type solutions under specific assumptions, its main contribution lies in explicitly incorporating structural knowledge into the variational functional, thereby modifying the inferential interpretation of extreme-event modelling. Rather than replacing existing statistical approaches, PCM offers a complementary perspective that articulates information theory, variational formulation, and hydrological modelling of extremes.

Appendix A: Main algorithms MIT-Q

MIT-Q comprises six modules. Module 1 simulates individual storm whose dynamics include a radial growth component and a second motion associated with advection by local winds over the DMQ. Its input consists of annual isohyets in raster format, and its output is a set of individual storm events grouped by year and characterized by the following parameters: longitude and latitude of the initiation centre; event duration DT (h); precipitation PRE (mm); shape exponent n; temporal exponent α_0; spatial exponent α_p; dominant-wind components Vx and Vy (km h^{-1}); radial celerity K (km h^{-1}); and the temporal hierarchical order of the rainfall bursts. Fig. A1 presents the model flowchart, whereas Figs. A2 and A3 highlight the temporal and spatial algorithms, respectively.

Module 2 provides a graphical user interface in which storms generated by Module 1 are simulated and rainfall intensities for different durations, as well as hyetographs from virtual stations, are extracted. The simulated rainfall intensities are compared with the official intensities in Ecuador using an Excel spreadsheet. This procedure feeds back into Module 1 until the model is fully calibrated and validated.

https://doi.org/10.5194/egusphere-2026-1317
Preprint. Discussion started: 8 April 2026

Module 3 simulates a virtual network of 2601 stations spaced 1 km apart (51 × 51). Based on the calibrated information, it extracts rainfall intensities at each station for durations between 5 min and 24 h, generating 2601 .txt files. Module 4 ranks, for each station, the maximum intensities in descending order. For a simulation equivalent to 500 years, Module 5 selects, at each station, values associated with specific return periods: the highest intensity as Tr = 500 years, the second as Tr = 250 years, and the tenth as Tr = 50 years. One file is generated for each return period and each duration, and the results are displayed in plots such as Fig. 6b. Finally, Module 6 uses the virtual hyetograph obtained as output from Module 2 and builds a database of the quartile in which the largest precipitation of each storm event is concentrated.

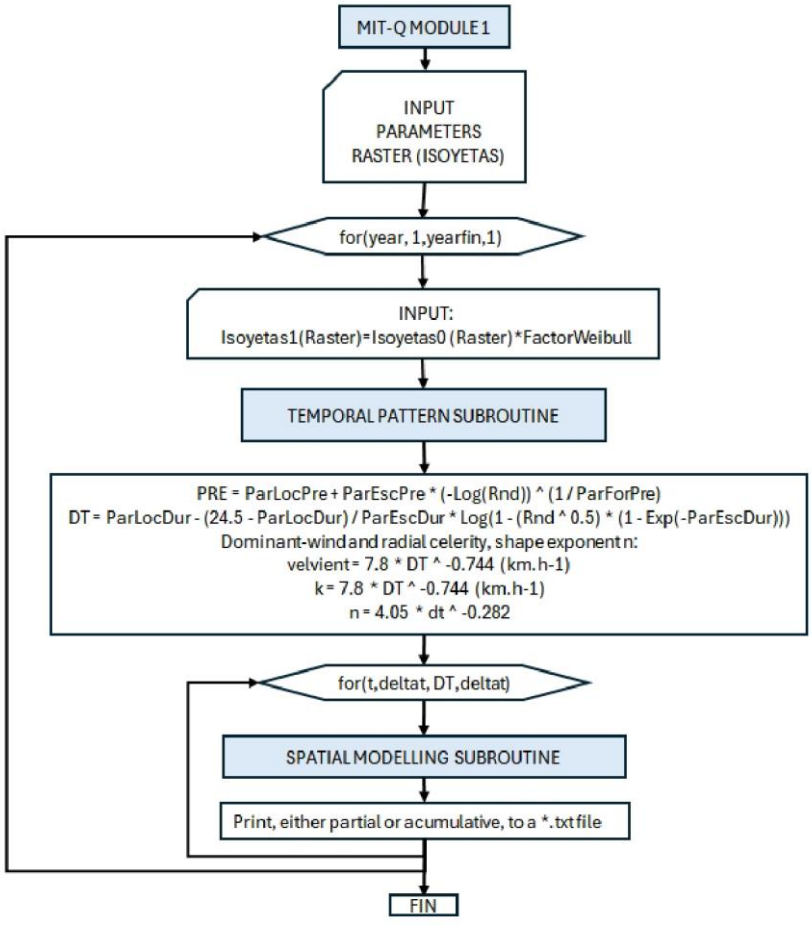

Figure A1. Flowchart of the MIT-Q model, showing the main modules and data flow used in storm simulation and post-processing.

https://doi.org/10.5194/egusphere-2026-1317
Preprint. Discussion started: 8 April 2026


```
TEMPORAL PATTERN SUBROUTINE
pa(0) = 0: pe(0) = 0
For j = 1 To m
        pa(j) = 1 / 2 * (1 - (Exp(-g / m)) ^ j) / (1 - Exp(-g)) + j / 2 / m
        ord(j) = j
Next j
For j = 1 To m
        pp(j) = pa(j) - pa(j - 1)
Next j
For i = 1 To m - 1
        ALEA = Rnd()
        For j = 1 To (m + 1 - i)
            If ALEA > pa(j - 1) And ALEA <= pa(j) Then
                ale(i) = ord(j)
                pe(i) = pe(i - 1) + pp(ale(i))
                jj = j
            End If
        Next j
        For j = jj To (m - i)
            ord(j) = ord(j + 1)
        Next j
        For j = 1 To (m - i)
            pa(j) = pa(j - 1) + pp(ord(j)) / (1 - pe(i))
        Next j
Next i
```

Figure A2. Temporal-modelling subroutine of MIT-Q, illustrating the intra-event temporal evolution of storm precipitation.

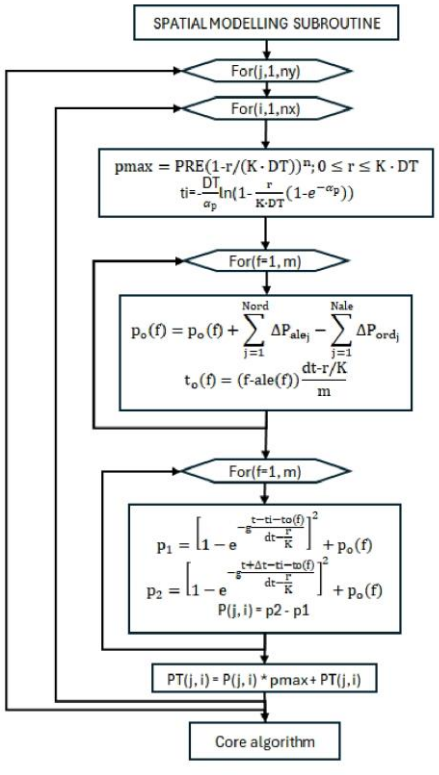

Figure A3. Spatial-modelling subroutine of MIT-Q, illustrating storm displacement and spatial rainfall distribution.

https://doi.org/10.5194/egusphere-2026-1317
Preprint. Discussion started: 8 April 2026

Code, data, or code and data availability

The data supporting this study are available on Zenodo at https://doi.org/10.5281/zenodo.18916818 (Beltrán Vega and Beltrán Valarezo, 2026). The source code for MIT-Q modules 1 and 2 can be made available by the corresponding author upon reasonable request, subject to a brief justification of the intended use.

Author contributions

The study was conceptualization by FB; AB developed the model code, performed the simulations and processed, analysed, and visualised the data. Both Authors contributed to data interpretation and to revising the manuscript.

Competing interests

The authors declare that they have no conflict of interest.

Acknowledgements

This work was initially carried out at the facilities of IDD. Consultores and later became part of the research advances of the Iddresearch.org group.
AI-assisted tools were used for language editing. The authors take full responsibility for the content of the manuscript.

Financial support

No external funding.

Review statement

The review statement will be added by Copernicus Publications.

References

Back, A. J.: Time distribution of heavy rainfall events in Urussanga, Santa Catarina State, Brazil, Acta Scientiarum. Agronomy, 33(4), 583–588, https://doi.org/10.4025/actasciagron.v33i4.6664, 2011

https://doi.org/10.5194/egusphere-2026-1317
Preprint. Discussion started: 8 April 2026

Barrera-Crespo, P. D., Langendoen, E. J., Ursic, M. E., Locke, M. A., Gibson, S., et al.: Major fluvial erosion and a 500-Mt sediment pulse triggered by lava-dam failure, Río Coca, Ecuador, Earth Surface Processes and Landforms, https://doi.org/10.1002/esp.5751, 2024.

Beltrán, A.: Modelo de Información de Tormentas MIT-Q (MIT-Q) (video), created in 2021, edited in 2024, IDD Research, available at: https://www.idd-research.org/modelo-de-informacion-de-tormentas-mit-q (last access: 7 March 2026), 2024.

Beltrán, F.: Lo que esconden las tormentas: Modelación espacio temporal de lluvias en el Ecuador, 1st edn., Autoedición, available at: https://www.amazon.com/-/es/Franklin-Aparicio-Beltran/dp/9942284133 (last access: 6 March 2026), 2017.

Beltrán, F.: Modelo de información de tormentas en Quito (MIT-Q), conference presented at Congreso Anual de Meteorología y Calidad del Aire CAMCA-2021, Quito, Ecuador, 17 Sep 2021, available at: https://www.usfq.edu.ec/sites/default/files/2021-08/libro-abstracts-camca-2021.pdf (last access: 6 March 2026), 2021.

Beltrán, F.: Un Principio de Certeza Máxima. Análisis Teórico de un Nuevo Invariante Probabilístico con Aplicaciones en el Estudio de Tormentas en Quito-Ecuador, Revista Politécnica, 52(2), 47–58, https://doi.org/10.33333/rp.vol52n2.05, 2023.

Beltrán Vega, F. A. and Beltrán Valarezo, A. J.: Data for: "Maximum Certainty Principle applied to rainfall modelling and regionalisation in Ecuador" (v1.0) [data set], Zenodo, https://doi.org/10.5281/zenodo.18916818, 2026.

Butterfield, J.: On symmetry and conserved quantities in classical mechanics, in: Physical theory and its interpretation, edited by: Demopoulos, W. and Pitowsky, I., Springer, 43–100, https://doi.org/10.1007/1-4020-4876-9_3, 2006.

Cosentino, P., Ficarra, V., and Luzio, D.: Truncated exponential frequency–magnitude relationship in earthquake statistics, Bulletin of the Seismological Society of America, 67(6), 1615–1623, available at: https://www.researchgate.net/publication/279463293 (last access: 6 March 2026), 1977.

Cover, T. M. and Thomas, J. A.: Elements of information theory, 2nd edn., Wiley, https://doi.org/10.1002/047174882X, 2006.

Crameri, F., Shephard, G. E., and Heron, P. J.: The misuse of colour in science communication, Nature Communications, 11, 5444, https://doi.org/10.1038/s41467-020-19160-7, 2020.

Empresa Metropolitana de Alcantarillado y Agua Potable [EMAAP-Q]: Normas de Diseño de Sistemas de Alcantarillado para la EPMAAP-Q, EPMAPS, available at: https://www.aguaquito.gob.ec/Alojamientos/PROYECTO%20LA%20MERCED/ANEXO%202%20NORMAS_ALCANTARILLADO_EMAAP.pdf (last access: 6 March 2026), 2009.

Escobar-González, D., Singaña-Chasi, M. S., González-Vergara, J., Erazo, B., Zambrano, M., Acosta, D., Villacís, M., Guallpa, M., Lahuatte, B., and Peluffo-Ordóñez, D. H.: Intensity–duration–frequency curve for extreme rainfall event characterization in the high tropical Andes, Water, 14(19), 2998, https://doi.org/10.3390/w14192998, 2022.

Garreaud, R. D.: The Andes climate and weather, Advances in Geosciences, 22, 3–11, https://doi.org/10.5194/adgeo-22-3-2009, 2009.

Guachamín, W., García, C., et al.: Determinación de Ecuaciones para el Cálculo de Intensidades Máximas de Precipitación, INAMHI, Quito, Ecuador, available at: https://www.inamhi.gob.ec/Publicaciones/Hidrologia/ESTUDIO_DE_INTENSIDADES_V_FINAL.pdf (last access: 6 March 2026), 2019.

Halder, A. K., Paliathanasis, A., and Leach, P. G. L.: Noether's theorem and symmetry, Symmetry, 10(12), 744, https://doi.org/10.3390/sym10120744, 2018.

https://doi.org/10.5194/egusphere-2026-1317
Preprint. Discussion started: 8 April 2026

Haviv, I., Enzel, Y., Whipple, K. X., Zilberman, E., Matmon, A., Stone, J., and Fifield, K. L.: Evolution of vertical knickpoints (waterfalls) with resistant caprock: Insights from numerical modeling, Journal of Geophysical Research: Earth Surface, 115(F3), F03028, https://doi.org/10.1029/2008JF001187, 2010.

Hosking, J. R. M. and Wallis, J. R.: Regional frequency analysis: An approach based on L-moments, Cambridge University Press, https://doi.org/10.1017/CBO9780511529443, 1997.

Huff, F.: Time distributions of heavy rain storms in Illinois, Illinois State Water Survey, 173, 1–18, available at: https://www.isws.illinois.edu/pubdoc/C/ISWSC-173.pdf (last access: 6 March 2026), 1990.

Huff, F. A.: Time distribution of rainfall in heavy storms, Water Resources Research, 3(4), 1007–1019, https://doi.org/10.1029/WR003i004p01007, 1967.

Jaynes, E. T.: Information theory and statistical mechanics, *Phys. Rev.*, 106, 620–630, https://doi.org/10.1103/PhysRev.106.620, 1957.

Kiran, K. and Mai, P.: Evidence for truncated exponential probability distribution of earthquake slip, Seismological Society of America, 106(4), 1802–1816, https://doi.org/10.1785/0120150291, 2016.

Kolmogorov, A. N.: Foundations of the theory of probability, 2nd English edn., edited by Morrison, N., Chelsea Publishing Company, New York, available at: https://www.york.ac.uk/depts/maths/histstat/kolmogorov_foundations.pdf (last access: 6 March 2026), 1956.

Kosmann-Schwarzbach, Y.: The Noether theorems: Invariance and conservation laws in the twentieth century, Springer, 57–62, https://doi.org/10.1007/978-0-387-87868-3, 2011.

Koutsoyiannis, D., Kozonis, D., and Manetas, A.: A mathematical framework for studying rainfall intensity–duration–frequency relationships, Journal of Hydrology, 206(1–2), 118–135, https://doi.org/10.1016/S0022-1694(98)00097-3, 1998.

Lévy-Leblond, J.-M.: Conceptos contrarios o el oficio de científico, transl. by Chabás Bergón, J., Tusquets, 2002.

NASA/METI/AIST/Japan Spacesystems and U.S./Japan ASTER Science Team: ASTER Global Digital Elevation Model V003 (ASTGTM.003) [data set], NASA Land Processes Distributed Active Archive Center (LP DAAC), https://doi.org/10.5067/ASTER/ASTGTM.003, 2019

Noether, E.: Invariante Variationsprobleme, Nachrichten von der Gesellschaft der Wissenschaften zu Göttingen, Mathematisch-Physikalische Klasse, 1918, 235–257, 1918.

Noether, E. and Tavel, M. A. (Trans.): Invariant variation problems, arXiv preprint, arXiv:physics/0503066, https://doi.org/10.48550/arXiv.physics/0503066, 2005.

Palacios, W., Zambrano, M., and Escobar, D.: Análisis temporal de las lluvias extremas en el DMQ y cálculo de las curvas de Intensidad-Duración-Frecuencia, EPMAPS, available at: https://www.aguaquito.gob.ec/Alojamientos/PALUGUILLO%20BELLAVISTA%20TRAMO%202/An%C3%A1lisis%20temporal%20de%20las%20lluvias%20extremas%20en%20el%20DMQ.pdf (last access: 6 March 2026), 2015.

Pourrut, P., et al.: El agua en El Ecuador: Clima, precipitaciones, escorrentía, Estudios de Geografía, 7, 86–87, available at: https://horizon.documentation.ird.fr/exl-doc/pleins_textes/pleins_textes_7/divers2/010014823.pdf (last access: 6 March 2026), 1995.

https://doi.org/10.5194/egusphere-2026-1317
Preprint. Discussion started: 8 April 2026

Pourrut, P. and Leiva, I.: Las lluvias de Quito: Características Generales, Beneficios y Problemática, in: Riesgos Naturales en Quito, Estudios de Geografía, Vol. 2, 34–44, available at: https://horizon.documentation.ird.fr/exl-doc/pleins_textes/divers11-10/31648.pdf (last access: 6 March 2026), 1989.

Rodríguez-Iturbe, I., Cox, D. R., and Isham, V.: Some models for rainfall based on stochastic point processes, Proceedings of the Royal Society of London. Series A, Mathematical and Physical Sciences, 410(1839), 269–288, https://doi.org/10.1098/rspa.1987.0039, 1987.

Shannon, C. E.: A mathematical theory of communication, Bell System Technical Journal, 27, 379–423, 623–656, https://doi.org/10.1002/j.1538-7305.1948.tb01338.x, 1948.

Traxl, D., Boers, N., Rheinwalt, A., Goswami, B., and Kurths, J.: The size distribution of spatiotemporal extreme rainfall clusters around the globe, Geophysical Research Letters, 43, 9939–9947, https://doi.org/10.1002/2016GL070692, 2016.